

Article

## 1,4,5-Trisubstituted Imidazole-Based p53-MDM2/MDMX Antagonists with Aliphatic Linkers for Conjugation with Biological Carriers

Aleksandra Twarda-Clapa, Sylwia Krzanik, Katarzyna Kubica, Katarzyna Guzik, Beata Labuzek, Constantinos G. Neochoritis, Kareem Khoury, Kaja Kowalska, Mirosława Czub, Grzegorz Dubin, Alexander Dömling, Lukasz Skalniak, and Tad A Holak

*J. Med. Chem.*, **Just Accepted Manuscript** • Publication Date (Web): 08 May 2017

Downloaded from <http://pubs.acs.org> on May 9, 2017

### Just Accepted

“Just Accepted” manuscripts have been peer-reviewed and accepted for publication. They are posted online prior to technical editing, formatting for publication and author proofing. The American Chemical Society provides “Just Accepted” as a free service to the research community to expedite the dissemination of scientific material as soon as possible after acceptance. “Just Accepted” manuscripts appear in full in PDF format accompanied by an HTML abstract. “Just Accepted” manuscripts have been fully peer reviewed, but should not be considered the official version of record. They are accessible to all readers and citable by the Digital Object Identifier (DOI®). “Just Accepted” is an optional service offered to authors. Therefore, the “Just Accepted” Web site may not include all articles that will be published in the journal. After a manuscript is technically edited and formatted, it will be removed from the “Just Accepted” Web site and published as an ASAP article. Note that technical editing may introduce minor changes to the manuscript text and/or graphics which could affect content, and all legal disclaimers and ethical guidelines that apply to the journal pertain. ACS cannot be held responsible for errors or consequences arising from the use of information contained in these “Just Accepted” manuscripts.

1  
2  
3  
4  
5  
6  
7  
8  
9  
10  
11  
12  
13  
14  
15  
16  
17  
18  
19  
20  
21  
22  
23  
24  
25  
26  
27  
28  
29  
30  
31  
32  
33  
34  
35  
36  
37  
38  
39  
40  
41  
42  
43  
44  
45  
46  
47  
48  
49  
50  
51  
52  
53  
54  
55  
56  
57  
58  
59  
60

# 1,4,5-Trisubstituted Imidazole-Based p53- MDM2/MDMX Antagonists with Aliphatic Linkers for Conjugation with Biological Carriers

*Aleksandra Twarda-Clapa,<sup>†,#</sup> Sylwia Krzanik,<sup>†,#</sup> Katarzyna Kubica,<sup>‡,#</sup> Katarzyna Guzik,<sup>‡</sup>  
Beata Labuzek,<sup>‡</sup> Constantinos G. Neochoritis,<sup>§</sup> Kareem Khoury,<sup>§</sup> Kaja Kowalska,<sup>||</sup> Mirosława  
Czub,<sup>‡</sup> Grzegorz Dubin,<sup>†,⊥</sup> Alexander Dömling,<sup>§</sup> Lukasz Skalniak,<sup>\*,‡</sup> and Tad A. Holak<sup>\*,‡,||,⊥</sup>*

<sup>†</sup> Faculty of Biochemistry, Biophysics and Biotechnology, Jagiellonian University,  
Gronostajowa 7, 30-387 Cracow, Poland

<sup>‡</sup> Faculty of Chemistry, Jagiellonian University, Ingardena 3, 30-060 Cracow, Poland

<sup>§</sup> Department of Drug Design, University of Groningen, Antonius Deusinglaan 1, 9700 AD  
Groningen, The Netherlands

<sup>||</sup> Max Plank Institute for Biochemistry, Am Klopferspitz 18, 82152 Martinsried, Germany

<sup>⊥</sup> Malopolska Centre of Biotechnology, Jagiellonian University, Gronostajowa 7a, 30-387  
Cracow, Poland

Keywords: p53, MDM2, MDMX, protein-protein interaction, inhibitor, dimerization, cancer

## ABSTRACT

The tumor suppressor protein p53, the “guardian of the genome”, is inactivated in nearly all cancer types by mutations in the *TP53* gene or by overexpression of its negative regulators, oncoproteins MDM2/MDMX. Recovery of p53 function by disrupting the p53-MDM2/MDMX interaction using small-molecule antagonists could provide an efficient non-genotoxic anticancer therapy. Here we present the syntheses, activities and crystal structures of the p53-MDM2/MDMX inhibitors based on the 1,4,5-trisubstituted imidazole scaffold which are appended with aliphatic linkers that enable coupling to bioactive carriers. The compounds have favorable properties at both biochemical and cellular levels. The most effective compound **19** is a tight binder of MDM2 and activates p53 in cancer cells that express the wild type p53, leading to cell cycle arrest and growth inhibition. Crystal structures reveal that compound **19** induces MDM2 dimerization *via* the aliphatic linker. This unique dimerization-binding mode opens new prospects for the optimization of the p53-MDM2/MDMX inhibitors and conjugation with bioactive carriers.

## INTRODUCTION

The tumor suppressor p53 is inactivated in the majority of human cancers, which is accomplished either by mutations in the *TP53* gene or by overexpression of p53 negative regulators, primarily MDM2 and/or MDMX.<sup>1-4</sup> Restoration of the function of p53 has been suggested as a promising strategy against cancer.<sup>1,2,5</sup> Mutations in the p53-encoding gene are found in about half of all human cancers and may be combated by gene therapy.<sup>6</sup> In the remaining 50% of cancer cases, in which wild type p53 (p53<sup>wt</sup>) is present, restoration of its activity by disrupting the interaction with MDM2/X proteins could be achieved by the use of small-molecule antagonists of the MDM2/MDMX-p53 interaction. It has been shown that such antagonists induce p53 downstream proteins, including p21, which leads to the induction

1  
2  
3 of the G0/G1 and G2/M cell cycle arrests and additionally induction of apoptosis in some  
4 cancer cell types.<sup>7-10</sup> Such an approach promises a broad range non-genotoxic therapy.<sup>1,11</sup>  
5  
6  
7  
8 Several classes of small-molecule MDM2 antagonists entered clinical trials.<sup>3,12-15</sup> However,  
9  
10 there are many challenges before entering clinical practice, mainly concerning  
11  
12 pharmacological properties, and a constant progress is needed to improve the potency of the  
13  
14 compounds and provide precise targeting of cancer cells.<sup>16-19</sup>  
15  
16

17  
18 The interaction of the N-terminal domain of MDM2 and MDMX with the N-terminal  
19  
20 transactivation domain of p53 is mediated by three key side chains of p53  $\alpha$ -helix: Phe19,  
21  
22 Trp23 and Leu26, which occupy hydrophobic subpockets on the MDM2 or MDMX  
23  
24 surface.<sup>20,21</sup> These interactions form a three finger pharmacophore, which is present in the  
25  
26 most of the currently available small-molecule MDM2 inhibitors.<sup>22,23</sup> Apart from this  
27  
28 canonical binding mode, several new approaches were recently proposed,<sup>24,25</sup> for instance  
29  
30 utilizing the transient states of MDM2 for the design of the small molecules occupying yet  
31  
32 another, fourth subpocket within MDM2 (inhibitor **YH300**, 3-(2-(tert-butylamino)-1-(N-(4-  
33  
34 (4-chlorobenzyloxy)benzyl)formamido)-2-oxoethyl)-6-chloro-1H-indole-2-carboxylic acid).<sup>26</sup>  
35  
36  
37  
38 A promising class of the p53-based stapled peptides have been recently proposed as another  
39  
40 novel group of antagonists.<sup>27,28</sup>  
41  
42

43  
44 Previously, we reported a novel compound based on an imidazole scaffold (6-chloro-3-(1-  
45  
46 (4-chlorobenzyl)-4-phenyl-1H-imidazol-5-yl)-1H-indole-2-carboxylic acid, **WK23**, named  
47  
48 thereafter **1.1**) and capable of disrupting the MDM2-p53 interaction *in vitro*.<sup>29</sup> In the present  
49  
50 study, we characterize compound **1** (Table 1), a derivative of **1.1**. Compared to **1.1**, the  
51  
52 derivatives of **1** have stronger binding to MDM2 and the improved p53-activating and  
53  
54 growth-inhibitory activities in cell-based assays. We also report a series of modifications of **1**  
55  
56 with aliphatic linkers at the carboxylic group that is attached to the indole ring system  
57  
58 (Table 1). This further improves biological properties of the derivatives of **1**. Our structure-  
59  
60

1  
2  
3 based analysis suggests the potential use of such aliphatic groups for conjugation of the  
4  
5  
6 compounds with biological carriers to improve solubility, stability and precise targeting to  
7  
8 malignant neoplasms.  
9

## 10 11 12 13 RESULTS AND DISCUSSION

14  
15 **Optimization of Compound 1.** In a previous study we identified **1** as one of the most  
16  
17 potent derivatives of **1.1** in disrupting the p53/MDM2 interaction in *in vitro* biochemical  
18  
19 assays.<sup>29</sup> Here we evaluate the activity of **1** in the cells and optimize its p53-activation,  
20  
21 growth-inhibitory and cell-cycle arrest properties by decorating the **1** scaffold (Table 1).  
22  
23

24  
25 Analyzing the co-crystal structure of **1.1** with MDM2, we identified position R<sub>2</sub> as a  
26  
27 potential site for compound expansion. The substituents at this position should point away  
28  
29 from the MDM2 molecule allowing for attachment of solubility/permeability enhancing  
30  
31 moieties or linkers for conjugation with targeting biological molecules, without significantly  
32  
33 affecting the affinity. Such assumptions were tested in compounds **13-19**.  
34  
35

36  
37 **1** was obtained in the three-component (3CR) van Leusen reaction (Figure 1).<sup>30</sup> Position R<sub>2</sub>  
38  
39 was modified to obtain both amide (**2-13**) and ester (**14-19**) derivatives using classical  
40  
41 chemistry (SI Schemes S1-S2, SI Tables S3-S4). Amide derivatives included two kinds of  
42  
43 substituents, polar groups expected to improve the pharmacokinetic properties of **1** and  
44  
45 aliphatic moieties tested to evaluate if additional binding at the surface of MDM2 may be  
46  
47 obtained. Ester derivatives included aliphatic linkers containing terminal reactive group  
48  
49 envisioned for future conjugation with biological carriers/targeting molecules. The binding of  
50  
51 selected derivatives was initially tested by NMR titration<sup>31,32</sup> and affinities (K<sub>i</sub>) of all  
52  
53 evaluated derivatives were tested by fluorescence polarization (FP) assay (Table 1, plots  
54  
55 presented in SI Table S5).  
56  
57  
58  
59  
60

1  
2  
3 Different modifications at R<sub>2</sub> position had different effects on the affinity towards MDM2,  
4 demonstrating that even though this substituent predictably should point away from the  
5 protein molecule, certain moieties were still poorly accepted. Modification with 4-  
6 morpholinopiperidinyl (**8**), 2-morpholinoethyl (**14**) or 6-succinyloxyhexyl (**16**) showed no  
7 negative effect on affinity. The binding of **3**, **4**, **6**, **18**, and **19** was slightly negatively affected,  
8 but the effect was negligible. The effect of other moieties was more pronounced with the  
9 affinities increasing above two digit nanomolar range (e.g. **2**, **5**, **7**, **9**, and **13**). Bulky  
10 substituents were not accepted at all at R<sub>2</sub> position (**10-12**). Both tested modification  
11 chemistries (amide vs ester) were compatible with MDM2 binding (e.g. **8** and **14**), although  
12 particular substituents favored certain chemistries as demonstrated by an order of magnitude  
13 better affinity of **14** compared to **13**. Since the modifications were introduced primarily with  
14 the aim of improving the effect of compounds on cells, all the derivatives which affinity was  
15 not significantly negatively affected were further evaluated in cellular assay as described  
16 below.

17  
18  
19  
20  
21  
22  
23  
24  
25  
26  
27  
28  
29  
30  
31  
32  
33  
34  
35  
36  
37  
38  
39  
40  
41  
42  
43  
44  
45  
46  
47  
48  
49  
50  
51  
52  
53  
54  
55  
56  
57  
58  
59  
60  
Potency of tested compounds towards MDMX followed the trend established for MDM2,  
although the affinities towards the former protein were around three orders of magnitude  
lower than those towards the latter as previously observed for **1.1**. **1** was the most potent  
MDMX binder with affinity (K<sub>i</sub>) of 3.15 μM. Clearly, despite significant homology of MDM2  
and MDMX, subtle differences in their p53 binding pockets<sup>33</sup> preclude optimization of **1**  
scaffold for concurrent binding to both those proteins.

Bista et al. have demonstrated that extending the Leu26-mimicking substituent within the  
three finger pharmacophore in the context of a 6-chloroindole scaffold opens an inducible  
noncanonical pocket by constraining Tyr100 in a position beneficial for binding larger  
substituents. Such four pocket binding mode was associated with improvement of affinity.<sup>26</sup>  
Here we tested if similar advantageous effect may be obtained within **1** scaffold. To this end

1  
2  
3 we introduced elongated benzyl amines in position R<sub>1</sub>. These modifications (**21-24**) resulted  
4  
5 in significant reduction of affinity towards MDM2 demonstrating that **1** scaffold is not suited  
6  
7 for exploring the noncanonical pocket observed by Bista et al.<sup>26</sup> Interestingly, in this  
8  
9 particular group of compounds the drop of affinity towards MDM2 was not associated with  
10  
11 significant change in potency against MDMX, again demonstrating differences in the p53  
12  
13 binding pockets of those two proteins.  
14  
15

16  
17 In parallel we evaluated the affinity of ethyl ester precursors (SI Table S2) of the **20-24**  
18  
19 series, but these compounds (**20a-24a**) have entirely lost their affinity both towards MDM2  
20  
21 and MDMX. This is relatively surprising given that the R<sub>2</sub> position is modified with much  
22  
23 larger substituents in **13-19**, but this phenomenon was not further evaluated in systematic  
24  
25 manner.  
26  
27

28  
29 **Derivatives of Compound 1 Induce p53-target Genes and Arrest the Cell Cycle.** The  
30  
31 on target effect of our 1,4,5-trisubstituted imidazoles in a biological context of a living cell  
32  
33 was evaluated by assessing the expression level of p53, MDM2 and p21 proteins, which are  
34  
35 the products of well-established p53 target genes. All compounds that had K<sub>i</sub> values in the FP  
36  
37 assay lower than 2 μM were tested. The second generation MDM2 antagonist **RG7388**  
38  
39 (Roche; 4-[(2R,3S,4R,5S)-3-(3-Chloro-2-fluoro-phenyl)-4-(4-chloro-2-fluorophenyl)-4-  
40  
41 cyano-5-(2,2-dimethyl-propyl)-pyrrolidine-2-carbonyl]-amino}-3-methoxybenzoic acid,  
42  
43 named thereafter **2.1**)<sup>34</sup> was used as a positive control. **2.1** induced expression of all of the  
44  
45 three proteins already 7 h after the treatment (Figures 2A,B). The densitometry analysis  
46  
47 revealed that the level of p21 expression was increased even stronger after 24 h of the  
48  
49 treatment (Figure 2C). Out of the tested compounds, **1**, **13**, **14**, **15**, **16**, and **19** induced  
50  
51 accumulations of p53, MDM2 and p21, suggesting the activation of the p53 pathway (Figures  
52  
53 2A,B, SI Figure S1). From these compounds, only for **13**, **14** and **19** the induction of p21  
54  
55  
56  
57  
58  
59  
60

1  
2  
3 expression was further increased at 24 h of the treatment as observed for **2.1**, possibly  
4 reflecting improved stability, retention or activity of the compounds in the cells (Figure 2C).  
5  
6

7  
8 In parallel, the off target effects/general toxicity were assessed by comparing the influence  
9 of tested agents on the viability of p53<sup>wt</sup> U-2 OS and p53-null Saos-2 cells. Accordingly, the  
10 compounds most active in the western blot analysis induced growth inhibition of U-2 OS  
11 (p53<sup>wt</sup>) cells at lower concentrations than the Saos-2 (p53<sup>-/-</sup>) cells suggesting on target effect  
12 (Table 2). Compound **15** revealed high toxicity towards Saos-2 cells and was removed from  
13 further analysis. As a control, nutlin-3 was used in the MTT assay, confirming its selectivity  
14 towards the p53<sup>wt</sup> cells (Table 2). The remaining tested compounds were disqualified due to  
15 their weak impact on the growth of the U-2 OS cell line (IC<sub>50</sub> values above 30 μM, e.g. **3**, **18**  
16 or **20**) or high toxicity towards the Saos-2 cells (selectivity lower than 1.5, e.g. **2**, **6** or **15**).  
17  
18  
19  
20  
21  
22  
23  
24  
25  
26  
27  
28

29 Accumulation of p21 upon activation of p53 is expected to trigger cell cycle arrest in the  
30 p53<sup>wt</sup> cells. The effect of the five most potent compounds on the cell cycle progression was  
31 tested in U-2 OS cells. Treatment with the 5 μM concentration of **13**, **14** or **19** resulted in a  
32 markedly decreased S-phase and increased G1 fraction (Figure 3). At higher concentrations  
33 (10 μM) **14** and **19** resulted in nearly complete depletion of the S-phase compartment, while  
34 for **1**, **16** and **13** the increase of the G1 fraction, in the expense of S phase, was clearly  
35 observed (Figure 3). The observed extent of cell cycle arrest was comparable to that obtained  
36 using 1 μM **2.1**, a compound currently undergoing clinical trials.  
37  
38  
39  
40  
41  
42  
43  
44  
45  
46  
47

48 Clearly, the selected compounds show the potency in blocking the progression of the cell  
49 cycle in a p53-dependent manner, and addition of the 2-morpholinoethyl or, especially, 6-  
50 succinyloxyhexyl substituent at position R<sub>2</sub> is profitable for the biological activity of  
51 compound **1**. In conclusion, compound **19** presents the best biological properties, as  
52 demonstrated by strong and sustained activation of p53-dependent expression of p21, the  
53  
54  
55  
56  
57  
58  
59  
60

1  
2  
3 highest selectivity in the MTT assay and the strongest induction of cell cycle arrest of p53<sup>wt</sup>  
4  
5 cells.  
6  
7

### 8 **Crystal Structure of MDM2-19 Complex Reveals Compound Induced Dimerization.**

9

10 In order to better understand the structural basis of the interactions of evaluated compounds at  
11 the binding pocket of MDM2, we determined the crystal structure of **19** in complex with the  
12 p53 binding domain of MDM2(18-125) (construct of MDM2 comprising residues 18-125). **19**  
13 was selected as the most efficient, cell-available, p53-activating derivative. At the same time  
14 the compound is potentially directly suitable for further conjugation with biological carriers  
15 for its reactive group at a long aliphatic linker.  
16  
17  
18  
19  
20  
21  
22  
23

24 The crystals diffracted to the 1.85 Å resolution and contained four protein molecules in the  
25 asymmetric unit. Each protein contained a single inhibitor molecule, all of which were well  
26 defined by their respective electron densities (SI Figure S2). No additional inhibitor molecules  
27 were found within the structure. In each case the inhibitor locates at the p53 binding pocket  
28 and occupies all the subpockets (Phe19, Trp23 and Leu26) of a canonical three-finger  
29 pharmacophore (Figure 4). The interaction of **19** with MDM2 is defined primarily by  
30 hydrophobic contacts. The 6-chloroindole substituent inserts into tryptophan pocket and  
31 assumes an orientation almost identical to the indole side chain in the native p53-MDM2  
32 complex while the chlorine atom potentiates the interaction at the bottom of the binding  
33 pocket. Further comparable to p53 interaction, the nitrogen within 6-chloroindole participates  
34 in a hydrogen bond with the carbonyl oxygen of Leu54. As such, the overall arrangement of  
35 6-chloroindole moiety follows a classical binding observed in a large number of MDM2  
36 inhibitors of different classes and repeating the indole interaction involved in p53 binding.<sup>16</sup>  
37  
38 4-chlorobenzyl substituent fills the Leu26 pocket in an orientation in which the chlorine atom  
39 points towards Tyr100. Phe19 pocket accommodates 4-fluorophenyl ring directed at Tyr67.  
40  
41  
42  
43  
44  
45  
46  
47  
48  
49  
50  
51  
52  
53  
54  
55  
56  
57  
58  
59  
60 The imidazole scaffold of **19** further contributes to the interaction by forming hydrophobic

1  
2  
3 contacts with Val93. As such, the binding of the core of the compound and aromatic  
4  
5 substituents is almost identical to that previously described for **1.1**. This is not surprising since  
6  
7  
8 **1.1** is a precursor of **19** (SI Figure S3).

9  
10 Most interesting are the interactions of the aliphatic linker unique to **19**. Comparable  
11  
12 affinities of **1** and **19** did not portend any pronounced protein – linker interactions. In fact, in  
13  
14 the crystal structure the linker protrudes outside the binding pocket. Only the disposition of  
15  
16 Gln72 and His73 sidechains differs from that observed in **1.1** containing structure. This  
17  
18 adjustment is necessary to accommodate the linker (SI Figure S3). Remarkably, however, the  
19  
20 protruding linker immediately contacts a second inhibitor molecule located within the  
21  
22 adjacent MDM2 molecule. The interaction is reciprocal as the linker of the inhibitor molecule  
23  
24 within the pocket of the adjacent MDM2 in turn contacts the inhibitor molecule within the  
25  
26 first MDM2. As such, the two MDM2 molecules form a dimer build around a dimer of two  
27  
28 inhibitor molecules (Figures 5A,B). The primary contacts between the inhibitor molecules  
29  
30 involve hydrogen bonds between the imidazole ring nitrogens and the nitrogens within the  
31  
32 aliphatic linker (Figure 5C). The overall dimer is further stabilized by reciprocal intra-MDM2  
33  
34 hydrogen bonds formed by Gln59 and Thr63 (Figure 5D). Moreover, the oxygen from the  
35  
36 carboxylic group terminating the aliphatic linker of each **19** molecule forms a water-mediated  
37  
38 contact with the side chains (Gln72, His96) of MDM2 (Figures 5A,C).

39  
40  
41 To test if the observed **19**-mediated MDM2(18-125) dimerization was unrelated to the lack  
42  
43 of the N-terminal part of the MDM2 domain in the evaluated construct we have solved the  
44  
45 crystal structure of **19** in complex with a different construct of MDM2(1-125). Moreover,  
46  
47 these crystals were obtained in different conditions and belonged to a different space group  
48  
49 providing a partial control of the influence of solvent conditions and crystal packing. Despite  
50  
51 these differences the dimerization mode within both structures is virtually identical,  
52  
53 suggesting that dimer formation is compound induced rather than an effect of particular  
54  
55  
56  
57  
58  
59  
60

1  
2  
3 experimental conditions. The MDM2 molecules within the dimers seen in the two crystal  
4 forms align with RMSD of 0.198 Å for corresponding C<sub>α</sub> atoms. The inhibitor dimers and  
5 interactions between the MDM2 molecules are also identical in both structures. The only  
6 difference is in amino acids 11-17 which were not present in the first construct, but are  
7 present and defined by electron density in the second structure. This fragment closes the  
8 binding pocket from both sides of the dimer (SI Figure S4), but has no significant effect on  
9 the mode of dimerization. Residues 1-10 were not defined by electron density.

10  
11  
12  
13  
14  
15  
16  
17  
18  
19  
20 Small molecule induced dimerization of MDM2 has already been previously reported by  
21 Graves et al. and by Surmiak et al., respectively for **RO-2443** (Roche; (Z)-5-((6-chloro-7-  
22 methyl-1H-indol-3-yl)methylene)-3-(3,4-difluorobenzyl)imidazolidine-2,4-dione, named  
23 thereafter **3.1**)<sup>35</sup> and 3-pyrrolin-2-ones/2-furanones.<sup>36</sup> In all instances the dimer is mediated by  
24 direct interaction of the inhibitor moieties facing outside of the binding pocket of MDM2.  
25 However, when the structures of **19**, **3.1** and 3-pyrrolin-2-ones/2-furanones induced dimers  
26 are compared by aligning one of the MDM2 molecules within the dimer, the positions of the  
27 partner molecules do not significantly overlap demonstrating different overall dimer  
28 arrangement (SI Figures S5-S6). The interactions between the inhibitor molecules are also  
29 significantly different. In **19**, it is the amide within the linker of one inhibitor molecule that  
30 forms a hydrogen bond with the nitrogen of the imidazole ring of adjacent inhibitor and *vice*  
31 *versa* (Figure 5). In **3.1**, aromatic stacking between the indolyl-hydantoin groups of adjacent  
32 inhibitors is primarily involved (SI Figure S5), whereas in 3-pyrrolin-2-ones/2-furanones it is  
33 a water mediated interaction between the inhibitor molecules and a halogen bond formed by  
34 the inhibitor and adjacent protein molecule (SI Figure S6).

35  
36  
37  
38  
39  
40  
41  
42  
43  
44  
45  
46  
47  
48  
49  
50  
51  
52  
53  
54  
55 Overall, although target protein dimerization through the interaction of exposed moieties of  
56 inhibitors is common for **19**, **3.1** and 3-pyrrolin-2-ones/2-furanones, the detailed molecular  
57 mechanisms and the overall geometry of the resulting dimers are largely dissimilar.  
58  
59  
60

### **19 Induces Dimerization of MDM2 in Solution and Dissociates p53-MDM2 Complex.**

The arrangement of the molecules in the crystal does not necessarily have to reflect the real biological assembly. Therefore, we evaluated if dimerization of MDM2 is induced by **19** in solution. The retention time characterizing MDM2 in analytical gel filtration decreased in the presence of **19** indicating formation of higher molecular weight species, presumably dimers (based on column calibration with globular protein standard). **19**-induced shifts in the elution volume were observed for all MDM2 constructs evaluated in this study (1-118, 1-125, 18-125; Figure 6A; SI Figure S7), so the observed dimerization is not induced by artificially exposing certain MDM2 surface.

Increase in the molecular mass of functional assembly results in increased relaxation time in NMR manifesting in signal broadening in the recorded spectra. To confirm **19**-induced dimerization of MDM2, the protein was titrated with the tested compound and the line width of well separated aliphatic signals in the region from -0.5 ppm to 1.0 ppm of 1D <sup>1</sup>H NMR spectra was monitored. Line width changes were not observed upon titration with **2.1**, a reference compound known not to affect the monomeric state of MDM2 in solution. Titration with **19** resulted in marked broadening of peaks indicating the dimerization (Figure 6B, SI Figure S7). Similar results were obtained regardless the MDM2 construct used (1-118, 18-125 and 1-125). These results further support the **19**-induced MDM2 dimerization in solution.

Next we asked if **19** is able to dissociate an existing p53-MDM2 complex. To test this, we employed a binding competition experiment, known as the 1D AIDA-NMR (Antagonist-Induced Dissociation Assay).<sup>37</sup> The method relies on monitoring the line width changes associated with the changes in the molecular weight upon complex formation. The well separated, sharp signal originating from Trp23 of p53 transactivation domain broadens to the level of noise upon binding to MDM2. Displacement of p53 peptide from MDM2 complex by an MDM2 inhibitor results in the recovery of the specific signal in 1D <sup>1</sup>H NMR spectrum.

1  
2  
3 Upon titration of p53-MDM2 complex with **19**, recovery of the specific Trp23 signal was  
4  
5 observed, demonstrating that the compound effectively dissociates the p53-MDM2 interaction  
6  
7 (Figure 6C), liberating p53 from the inhibition by its negative regulator.  
8  
9

## 17 CONCLUSIONS

19  
20 Derivatization of the previously reported **1.1**, first into compound **1** and later by modification  
21  
22 of the carboxyl moiety of the chloroindole scaffold, has led to a number of compounds with  
23  
24 affinities comparable to the starting structure, but characterized by significantly improved  
25  
26 activity in cell based assays. The best obtained compounds activated p53 in cancer cells to the  
27  
28 level comparable to the golden standard–nutlin-3a, that is induced the cell cycle arrest,  
29  
30 increased the expression of proapoptotic p21 and had a markedly increased cytotoxicity  
31  
32 towards p53 positive cells. Crystal structure of an example compound (**19**) revealed a  
33  
34 classical three finger pharmacophore binding mode identical to that of **1.1**, but at the same  
35  
36 time an unexpected, inhibitor induced dimerization of the target protein. The dimerization was  
37  
38 confirmed in solution. Such unusual binding mode provides entirely new repertoire of  
39  
40 optimization possibilities. Further, the long aliphatic linkers, containing functional groups,  
41  
42 allow for future attachment of presented series of compounds to biological carriers (e.g.  
43  
44 hyaluronic acid)<sup>38</sup> for improved pharmacodynamics and better delivery.  
45  
46  
47  
48  
49  
50  
51  
52

## 53 EXPERIMENTAL SECTION

54  
55 **Synthesis.** Compounds **1** and **20-24** were obtained in the 3CR van Leusen reaction. **1** was  
56  
57 further modified at position R<sub>2</sub> to obtain amide (**2-13**) and ester (**14-19**) derivatives using  
58  
59 classical chemistry. The purity of all final compounds - determined by the chromatographic  
60

1  
2  
3 UPLC or elemental analysis - was 95% or higher. For details of synthesis and analysis, see  
4  
5 the SI.  
6

7  
8 **Protein Expression and Purification.** Variants of the N-terminal domain of human  
9  
10 MDM2 (1-118; 1-125 and 18-125) were cloned into the pET-20 (Novagen) and expressed in  
11  
12 *E. coli* strain BL21-CodonPlus(DE3)-RIL as described previously.<sup>39</sup> In brief, cells were  
13  
14 cultured at 37°C. Protein expression was induced with 1 mM IPTG at OD<sub>600</sub> of 0.8 and  
15  
16 cultured for additional 5 h at 37°C. Cells were collected by centrifugation and lysed by  
17  
18 sonication. Inclusion bodies were collected by centrifugation, washed with PBS containing  
19  
20 0.05% Triton-X100 and subsequently solubilized in 6 M guanidine hydrochloride in 100 mM  
21  
22 Tris-HCl, pH 8.0, containing 1 mM EDTA and 10 mM β-mercaptoethanol. The protein was  
23  
24 dialyzed against 4 M guanidine hydrochloride pH 3.5 supplemented with 10 mM β-  
25  
26 mercaptoethanol. Following, the protein was refolded by dropwise addition into 10 mM Tris-  
27  
28 HCl, pH 7.0, containing 1 mM EDTA and 10 mM β-mercaptoethanol and slow mixing  
29  
30 overnight at 4°C. Ammonium sulfate was added to the final concentration of 1.5 M and the  
31  
32 refolded protein was recovered on Butyl Sepharose 4 Fast Flow (GE Healthcare). The protein  
33  
34 was eluted using 100 mM Tris-HCl pH 7.2 containing 5 mM β-mercaptoethanol and further  
35  
36 purified by gel filtration on HiLoad 16/600 S75 (GE Healthcare) in 5 mM Tris-HCl pH 8.0  
37  
38 containing 50 mM NaCl and 5 mM β-mercaptoethanol (crystallization buffer) or in 50 mM  
39  
40 phosphate buffer pH 7.4 containing 150 mM NaCl and 5 mM DTT (FP/NMR buffer).  
41  
42  
43  
44  
45  
46  
47

48 N-terminal domain of human MDMX (1-134) was cloned into pET-46Ek/LIC vector  
49  
50 (Novagen). The vector was transformed into *E. coli* strain BL21-CodonPlus(DE3)-RIL cells.  
51  
52 The cells were cultured at 37°C and protein expression was induced with 0.5 mM IPTG at  
53  
54 OD<sub>600</sub> nm of 0.6. The recombinant protein expression was carried for 12 h at 20°C. The  
55  
56 protein was purified in native conditions by metal affinity chromatography. The preparation  
57  
58  
59  
60

1  
2  
3 was polished by gel filtration on HiLoad 16/600 S75 (GE Healthcare) in 50 mM phosphate  
4 buffer pH 7.4 containing 150 mM NaCl and 5 mM DTT (FP/NMR buffer).  
5  
6  
7

8 **Fluorescence Polarization Assay.** The assay was performed in 50 mM NaCl, 10 mM Tris  
9 pH 8.0, 1 mM EDTA containing 5% DMSO. To determine the optimal concentration of the  
10 protein for the competition binding assay, the effective concentration of MDM2 (1-118) and  
11 MDMX (1-134) was each time ascertained by determining the apparent  $K_d$  towards 5'-FAM-  
12 LTFEHYWAQLTS (P2; 10 nM). Competition assay was performed by contacting serial  
13 dilutions of tested compounds with 10 nM P2 at protein concentration yielding  $f_0=0.8$ .<sup>40</sup>  
14  
15  
16  
17  
18  
19  
20  
21  
22  
23  
24  
25  
26  
27  
28  
29  
30  
31  
32  
33  
34  
35  
36  
37  
38  
39  
40  
41  
42  
43  
44  
45  
46  
47  
48  
49  
50  
51  
52  
53  
54  
55  
56  
57  
58  
59  
60  
Fluorescence polarization was determined at 485 nm excitation and 535 nm emission 15 min  
after mixing all assay components. All tests were performed using Corning black 96-well  
NBS assay plates at room temperature.

30  
31  
32  
33  
34  
35  
36  
37  
38  
39  
40  
41  
42  
43  
44  
45  
46  
47  
48  
49  
50  
51  
52  
53  
54  
55  
56  
57  
58  
59  
60  
**Cell Lines and Treatment with Compounds.** U-2 OS (p53<sup>wt</sup>), HCT 116 (p53<sup>wt</sup>) and  
Saos-2 (p53<sup>-/-</sup>) cells were cultured as monolayers in McCoy's 5A Medium containing L-  
glutamine (Lonza) and supplemented with 10% fetal bovine serum (Biowest) at 37°C and 5%  
CO<sub>2</sub> in a humidified atmosphere. All compounds were prepared as 50 mM stock solutions in  
DMSO. The cells were exposed to the inhibitors for indicated time periods. In each  
experiment, the final concentration of DMSO was kept constant and below detectable effect  
level.

46  
47  
48  
49  
50  
51  
52  
53  
54  
55  
56  
57  
58  
59  
60  
**Western Blot Analysis.** U-2 OS cells and HCT 116 cells (120 000 cells per well) were  
seeded on 12-well transparent plates (Falcon). The inhibitors were added 24 h following  
seeding and the cells were cultured for additional 7 or 24 h. Cells were lysed with RIPA  
buffer (Sigma) supplemented with protease inhibitor cocktail (Sigma). The protein lysate was  
clarified by centrifugation and analyzed on 12% SDS polyacrylamide gel (Bio-Rad). The  
proteins were transferred to PVDF membrane (Merck Millipore). The membranes were  
blocked for 1 h in 5% BSA (Bioshop) in TTBS (100 mM Tris-HCl pH 8.0 containing 0.05%

1  
2  
3 Tween-20 and 150 mM NaCl). Blots were probed with following antibodies: anti-MDM2  
4  
5 (Thermo Fisher Scientific, cat. no. 700555), p21 (Cell Signaling, cat. no. 2947), both at  
6  
7 1:2000 dilution, anti-p53 (Santa Cruz Biotechnology, cat. no. sc-6243) at 1:200 dilution or  
8  
9 anti-GAPDH (Cell Signaling, cat. no. 2118) at 1:3000 dilution. Anti-rabbit antibody  
10  
11 conjugated with horseradish peroxidase (Cell Signaling, cat. no. 7074) at 1:3000 dilution was  
12  
13 used to detect the primary antibodies. The blots were developed using ECL Western Blotting  
14  
15 KIT (Bio-Rad) and visualized using ChemiDoc System (Bio-Rad). Densitometric analysis  
16  
17 was performed using ImgeLab software (Bio-Rad).  
18  
19  
20  
21

22 **Cell Viability Assay.** U-2 OS cells (500 cells per well) and Saos-2 cells (1500 cells per  
23  
24 well) were seeded on 96-well transparent plates (Falcon). Cells were treated with inhibitors  
25  
26 24 h following the seeding and cultured for additional 5 days. Thiazolyl blue tetrazolium  
27  
28 bromide (MTT) was added at the final concentration of 500 ng mL<sup>-1</sup> and the cells were  
29  
30 incubated for 1 h at 37°C. The medium was removed and formazan crystals were dissolved in  
31  
32 isopropanol containing 40 mM HCl. Absorbance was determined at 570 nm relative to  
33  
34 650 nm reference. Data was normalized to DMSO-treated control. Data was analyzed using  
35  
36 Origin software (OriginLab). IC<sub>50</sub> values were calculated by fitting of 'Dose Resp' curves to  
37  
38 experimental datasets.  
39  
40  
41  
42

43 **Cell Cycle Analysis.** U-2 OS cells were seeded at 300 000 per 60·15 mm cell culture dish  
44  
45 (Eppendorf), treated with tested inhibitors for 24 h, trypsinized and fixed with 70% ethanol.  
46  
47 The cell concentration was adjusted to 1 x 10<sup>6</sup> cells/sample and DNA was labeled with PI-  
48  
49 RNase solution (PBS, 5 µg mL<sup>-1</sup> propidium iodide, 0.01 mg mL<sup>-1</sup> RNase A) for 30 min at  
50  
51 25°C. The cells analyzed for cell cycle DNA content using LSRFortessa cell analyzer (BD  
52  
53 Biosciences).  
54  
55  
56  
57

58 **Crystal Structure Determination.** Human MDM2 (residues 18-125 and 1-125) was  
59  
60 prepared in 5 mM Tris-HCl pH 8.0 containing 50 mM NaCl and 5 mM β-mercaptoethanol.

1  
2  
3 Molar excess (3×) of **19** was added and the complex was concentrated to 20 mg mL<sup>-1</sup>.  
4  
5 Screening for crystallization conditions was performed using sitting drop vapor diffusion  
6  
7 setup and commercially available buffer sets (Qiagen, Hampton Research). Crystals of the  
8  
9 MDM2(18-125)-**19** complex appeared after few days at 4°C in 0.1 M Na HEPES pH 7.5  
10  
11 containing 10% isopropanol and 20% PEG 4000. The MDM2(1-125)-**19** complex crystallized  
12  
13 at 4°C in 0.1 M HEPES pH 7.5 containing 0.2 M NaCl and 25% PEG 3350. The data  
14  
15 collection and refinement description and statistics (SI Table S6) are summarized in the SI.  
16  
17  
18

19  
20 **Analytical Gel Filtration.** MDM2(18-125, 1-118 and 1-125) at 1 mg mL<sup>-1</sup> was contacted  
21  
22 with 3× molar excess of tested inhibitor for 30 min and the distribution on different molecular  
23  
24 weight species was analyzed by gel filtration in the crystallization buffer using S75 10/300  
25  
26 GL column (GE Healthcare).  
27  
28

29  
30 **NMR Experiments.** All NMR spectra were acquired at 300 K using a Bruker Avance 600  
31  
32 MHz spectrometer. Uniform <sup>15</sup>N isotope labelling was achieved by expression of the protein  
33  
34 in the M9 minimal medium containing <sup>15</sup>NH<sub>4</sub>Cl as the sole nitrogen source. MDM2(1-  
35  
36 118)<sup>41,42</sup> was prepared in 50 mM phosphate buffer pH 7.4 containing 150 mM NaCl and  
37  
38 5 mM DTT. 10% (v/v) of D<sub>2</sub>O was added to the samples to provide lock signal. Water  
39  
40 suppression was carried out using the WATERGATE sequence.<sup>43</sup> Stock solutions of  
41  
42 inhibitors used for titration were prepared in d<sub>6</sub>-DMSO. The spectra were processed with  
43  
44 TopSpin 3.2 software. <sup>1</sup>H-<sup>15</sup>N heteronuclear correlations were obtained using the fast HSQC  
45  
46 pulse sequence.<sup>44</sup> Assignment of the amide groups of MDM2 was obtained after <sup>45</sup>.  
47  
48  
49 The AIDA experiments were performed according to <sup>37</sup>.  
50  
51  
52  
53  
54

## 55 ASSOCIATED CONTENT

### 56 Supporting Information

57  
58  
59  
60

1  
2  
3 Details on chemical synthesis of compounds, X-ray, FP and NMR may be found in the  
4  
5 Supporting Information. This material as well as Molecular Formula Strings are available free  
6  
7 of charge via the Internet at <http://pubs.acs.org>.  
8  
9

### 10 Accession Codes

11  
12 The final models and structure factors for MDM2-**19** complexes were deposited into Protein  
13  
14 Data Bank with the following accession numbers: 5J7G (MDM2 18-125) and 5J7F (MDM2  
15  
16 1-125).  
17  
18  
19  
20  
21

### 22 AUTHOR INFORMATION

#### 23 Corresponding Author

24  
25  
26 \* T. A. Holak: [holak@biochem.mpg.de](mailto:holak@biochem.mpg.de), +48 126632287; L. Skalniak:  
27  
28 lukasz.skalniak@uj.edu.pl, +48 126632041.  
29  
30

#### 31 Author Contributions

32  
33  
34 # These authors contributed equally to this work.  
35

#### 36 Notes

37  
38 The authors declare no competing financial interest.  
39  
40  
41  
42

### 43 ACKNOWLEDGMENTS

44  
45 This research has been supported (to TAH) by the Maestro grant UMO-2012/06/A/ST5/00224  
46  
47 from the National Science Centre, Poland, by the Project operated within the Foundation for  
48  
49 Polish Science TEAM Program, co-financed by the EU European Regional Development  
50  
51 Fund and the Marie Curie FP7-Reintegration-Grant within the 7th European Community  
52  
53 Framework Programme and (to GD) UMO-2011/01/D/NZ1/01169 from the National Science  
54  
55 Centre. ATC was supported by Preludium grant UMO-2015/17/N/NZ1/00025, KK - by  
56  
57 Preludium grant UMO-2015/17/N/ST5/01942, LS - by Sonata grant UMO-  
58  
59  
60

1  
2  
3 2016/21/D/NZ7/00596 and GD - by Sonata bis grant UMO-2012/07/E/NZ1/01907 from the  
4  
5 National Science Centre, Poland. AD was supported by the NIH (1R21GM087617,  
6  
7 1R01GM097082, and 1P41GM094055). The research was carried out with the equipment  
8  
9 purchased thanks to the financial support of the European Union structural funds (contract no.  
10  
11 POIG.02.01.00-12-064/08 and POIG.02.01.00-12-167/08) and European Regional  
12  
13 Development Fund in the framework of the Polish Innovation Economy Operational Program  
14  
15 (contract no. POIG.02.01.00-12-023/08). This project has received funding from the European  
16  
17 Union's Framework Programme for Research and Innovation Horizon 2020 (2014-2020)  
18  
19 under the Marie Skłodowska-Curie Grant Agreement No. 675555, Accelerated Early staGe  
20  
21 drug discovery (AEGIS). SK received the financial support from the Faculty of Biochemistry,  
22  
23 Biophysics and Biotechnology of Jagiellonian University, a partner of the Leading National  
24  
25 Research Center (KNOW) supported by the Ministry of Science and Higher Education.  
26  
27  
28  
29  
30  
31  
32  
33

#### 34 **ABBREVIATIONS USED**

35  
36  
37 3CR, 3-Component Reaction; AIDA, Antagonist-Induced Dissociation Assay; FP,  
38  
39 Fluorescence Polarization; GAPDH, Glyceraldehyde-3-Phosphate Dehydrogenase; MTT, 3-  
40  
41 (4,5-Dimethylthiazol-2-yl)-2,5-Diphenyltetrazolium Bromide; MDM2, Murine Double  
42  
43 Minute-2; MDMX, Murine Double Minute-X; PVDF, Polyvinylidene Fluoride; RMSD, Root  
44  
45 Mean Square Deviation.  
46  
47  
48  
49  
50  
51

#### 52 **REFERENCES**

53  
54  
55 (1) Brown, C. J.; Lain, S.; Verma, C. S.; Fersht, A. R.; Lane, D. P. Awakening guardian  
56  
57 angels: drugging the p53 pathway. *Nat. Rev. Cancer* **2009**, *9*, 862–873.  
58  
59  
60

1  
2  
3 (2) Cheok, C. F.; Verma, C. S.; Baselga, J.; Lane, D. P. Translating p53 into the clinic. *Nat.*  
4  
5 *Rev. Clin. Oncol.* **2011**, *8*, 25–37.

6  
7  
8  
9 (3) Wade, M.; Li, Y. C.; Wahl, G. M. MDM2, MDMX and p53 in oncogenesis and cancer  
10  
11 therapy. *Nat. Rev. Cancer* **2013**, *13*, 83–96.

12  
13  
14 (4) Hock, A. K.; Vousden, K. H. The role of ubiquitin modification in the regulation of  
15  
16 p53. *Biophys. Acta* **2014**, *1843*, 137–149.

17  
18  
19  
20 (5) Karni-Schmidt, O.; Lokshin, M.; Prives, C. The roles of MDM2 and MDMX in cancer.  
21  
22 *Annu. Rev. Pathol. Mech. Dis.* **2016**, *11*, 617–644.

23  
24  
25 (6) Gu, J.; Wang, B.; Liu, Y.; Zhong, L.; Tang, Y.; Guo, H.; Jiang, T.; Wang, L.; Li, Y.;  
26  
27 Cai, L. Murine double minute 2 siRNA and wild-type p53 gene therapy interact positively  
28  
29 with zinc on prostate tumours in vitro and in vivo. *Eur. J. Cancer* **2014**, *50*, 1184–1194.

30  
31  
32  
33 (7) Shangary, S.; Qin, D.; McEachern, D.; Liu, M.; Miller, R. S.; Qiu, S.; Nikolovska-  
34  
35 Coleska, Z.; Ding, K.; Wang, G.; Chen, J.; Bernard, D.; Zhang, J.; Lu, Y.; Gu, Q.; Shah, R.  
36  
37 B.; Pienta, K. J.; Ling, X.; Kang, S.; Guo, M.; Sun, Y.; Yang, D.; Wang, S. Temporal  
38  
39 activation of p53 by a specific MDM2 inhibitor is selectively toxic to tumors and leads to  
40  
41 complete tumor growth inhibition. *Proc. Natl. Acad. Sci. U. S. A.* **2008**, *105*, 3933–3938.

42  
43  
44  
45 (8) Miyachi, M.; Kakazu, N.; Yagyu, S.; Katsumi, Y.; Tsubai-Shimizu, S.; Kikuchi, K.;  
46  
47 Tsuchiya, K.; Iehara, T.; Hosoi, H. Restoration of p53 pathway by nutlin-3 induces cell cycle  
48  
49 arrest and apoptosis in human rhabdomyosarcoma cells. *Clin. Cancer Res.* **2009**, *15*, 4077–  
50  
51 4084.

52  
53  
54  
55 (9) Chen, L.; Rousseau, R. F.; Middleton, S. A.; Nichols, G. L.; Newell, D. R.; Lunec, J.;  
56  
57 Tweddle, D. A. Pre-clinical evaluation of the MDM2-p53 antagonist RG7388 alone and in  
58  
59 combination with chemotherapy in neuroblastoma. *Oncotarget* **2015**, *6*, 10207–10221.  
60

1  
2  
3 (10) Feng, F. Y.; Zhang, Y.; Kothari, V.; Evans, J. R.; Jackson, W. C.; Chen, W.; Johnson,  
4 S. B.; Luczak, C.; Wang, S.; Hamstra, D. A. MDM2 inhibition sensitizes prostate cancer cells  
5 to androgen ablation and radiotherapy in a p53-dependent manner. *Neoplasia* **2016**, *18*, 213–  
6 222.  
7

8  
9  
10  
11  
12 (11) Vassilev, L. T.; Vu, B. T.; Graves, B.; Carvajal, D.; Podlaski, F.; Filipovic, Z.; Kong,  
13 N.; Kammlott, U.; Lukacs, C.; Klein, C.; Fotouhi, N.; Liu E. A. In vivo activation of the p53  
14 pathway by small-molecule antagonists of MDM2. *Science* **2004**, *303*, 844–848.  
15  
16  
17

18  
19 (12) Hoe, K. K.; Verma, C. S.; Lane, D. P. Drugging the p53 pathway: understanding the  
20 route to clinical efficacy. *Nat. Rev. Drug Discovery*. **2014**, *13*, 217–236.  
21  
22  
23

24  
25 (13) Zhao, Y.; Aguilar, A.; Bernard, D.; Wang, S. Small-molecule inhibitors of the  
26 MDM2-p53 protein-protein interaction (MDM2 Inhibitors) in clinical trials for cancer  
27 treatment. *J. Med. Chem.* **2015**, *58*, 1038–1052.  
28  
29  
30  
31

32  
33 (14) Burgess, A.; Chia, K. M.; Haupt, S.; Thomas, D.; Haupt, Y.; Lim, E. Clinical  
34 overview of MDM2/X-targeted therapies. *Front Oncol.* **2016**, *6*, 7.  
35  
36  
37  
38

39  
40 (15) Urso, L.; Calabrese, F.; Favaretto, A.; Conte, P.; Pasello, G. Critical review about  
41 MDM2 in cancer: Possible role in malignant mesothelioma and implications for treatment.  
42 *Crit Rev Oncol Hematol.* **2016**, *97*, 220–230.  
43  
44  
45  
46

47  
48 (16) Popowicz, G. M.; Dömling, A.; Holak, T. A. The structure-based design of  
49 Mdm2/Mdmx-p53 inhibitors gets serious. *Angew. Chem., Int. Ed.* **2011**, *50*, 2680–2688.  
50  
51  
52

53  
54 (17) Uversky, V. N.; Dave, V.; Iakoucheva, L. M.; Malaney, P.; Metallo, S. J.; Pathak, R.  
55 R.; Joerger, A. C. Pathological unfoldomics of uncontrolled chaos: intrinsically disordered  
56 proteins and human diseases. *Chem. Rev.* **2014**, *114*, 6844–6879.  
57  
58  
59  
60

1  
2  
3 (18) Milroy, L. G.; Grossmann, T. N.; Hennig, S.; Brunsveld, L.; Ottmann, C. Modulators  
4 of protein–protein interactions. *Chem. Rev.* **2014**, *114*, 4695–4748.  
5  
6

7  
8  
9 (19) Pelay-Gimeno, M.; Glas, A.; Koch, O.; Grossmann, T. N. Structure-based design of  
10 inhibitors of protein-protein interactions: mimicking peptide binding epitopes. *Angew. Chem.,*  
11 *Int. Ed.* **2015**, *54*, 8896–8927.  
12  
13  
14

15  
16  
17 (20) Kussie, P. H.; Gorina, S.; Marechal, V.; Elenbaas, B.; Moreau, J.; Levine, A. J.;  
18 Pavletich, N. P. Structure of the MDM2 oncoprotein bound to the p53 tumor suppressor  
19 transactivation domain. *Science* **1996**, *274*, 948–953.  
20  
21  
22

23  
24  
25 (21) Joerger, A. C.; Fersht, A. R. The p53 pathway: origins, inactivation in cancer, and  
26 emerging therapeutic approaches. *Annu. Rev. Biochem.* **2016**, *85*, 375–404.  
27  
28  
29

30  
31 (22) Ding, K.; Lu, Y.; Nikolovska-Coleska, Z.; Qiu, S.; Ding, Y.; Gao, W.; Stuckey, J.;  
32 Krajewski, K.; Roller, P. P.; Tomita, Y.; Parrish, D. A.; Deschamps, J. R.; Wang, S.  
33 Structure-based design of potent non-peptide MDM2 inhibitors. *J. Am. Chem. Soc.* **2005**, *127*,  
34 10130–10131.  
35  
36  
37  
38

39  
40  
41 (23) Ding, K.; Lu, Y.; Nikolovska-Coleska, Z.; Wang, G.; Qiu, S.; Shangary, S.; Gao, W.;  
42 Qin, D.; Stuckey, J.; Krajewski, K.; Roller P. P.; Wang S. Structure-based design of spiro-  
43 oxindoles as potent, specific small-molecule inhibitors of the MDM2-p53 interaction. *J. Med.*  
44 *Chem.* **2006**, *49*, 3432–3435.  
45  
46  
47  
48

49  
50  
51 (24) Michelsen, K.; Jordan, J. B.; Lewis, J.; Long, A. M.; Yang, E.; Rew, Y.; Zhou, J.;  
52 Yakowec, P.; Schnier, P. D.; Huang, X.; Poppe, L. Ordering of the N-terminus of human  
53 MDM2 by small molecule inhibitors. *J. Am. Chem. Soc.* **2012**, *134*, 17059–17067.  
54  
55  
56  
57  
58  
59  
60

1  
2  
3 (25) Vogel, S. M.; Bauer, M. R.; Joerger, A. C.; Wilcken, R.; Brandt, T.; Veprintsev, D.  
4  
5 B.; Rutherford, T. J.; Fersht, A. R.; Boeckler, F. M. Lithocholic acid is an endogenous  
6  
7 inhibitor of MDM4 and MDM2. *Proc. Natl. Acad. Sci. U. S. A.* **2012**, *109*, 16906–16910.  
8  
9

10  
11 (26) Bista, M.; Wolf, S.; Khoury, K.; Kowalska, K.; Huang, Y.; Wrona, E.; Arciniega, M.;  
12  
13 Popowicz, G. M.; Holak, T. A.; Dömling, A. Transient protein states in designing inhibitors  
14  
15 of the MDM2-p53 interaction. *Structure* **2013**, *21*, 2143–2151.  
16  
17

18  
19 (27) Baek, S.; Kutchukian, P. S.; Verdine, G. L.; Huber, R.; Holak, T. A.; Lee, K. W.;  
20  
21 Popowicz, G. M. Structure of the stapled p53 peptide bound to Mdm2. *J. Am. Chem. Soc.*  
22  
23 **2012**, *134*, 103–106.  
24  
25

26  
27 (28) Chang, Y.S.; Graves, B.; Guerlavais, V.; Tovar, C.; Packman, K.; To, K.H.; Olson, K.  
28  
29 A.; Kesavan, K.; Gangurde, P.; Mukherjee, A.; Baker, T.; Darlak, K.; Elkin, C.; Filipovic, Z.;  
30  
31 Qureshi, F. Z.; Cai, H.; Berry, P.; Feyfant, E.; Shi, X. E.; Horstick, J.; Annis, D. A.; Manning,  
32  
33 A. M.; Fotouhi, N.; Nash, H.; Vassilev, L. T.; Sawyer, T. K. Stapled  $\alpha$ -helical peptide drug  
34  
35 development: a potent dual inhibitor of MDM2 and MDMX for p53-dependent cancer  
36  
37 therapy. *Proc. Natl. Acad. Sci. U. S. A.* **2013**, *110*, E3445–E3454.  
38  
39  
40

41  
42 (29) Popowicz, G.M.; Czarna, A.; Wolf, S.; Wang, K.; Wang, W.; Dömling, A.; Holak, T.  
43  
44 A. Structures of low molecular weight inhibitors bound to MDMX and MDM2 reveal new  
45  
46 approaches for p53-MDMX/MDM2 antagonist drug discovery. *Cell Cycle* **2010**, *9*, 1104–  
47  
48 1111.  
49

50  
51  
52 (30) Dömling, A.; Wang, W.; Wang, K. Chemistry and biology of multicomponent  
53  
54 reactions. *Chem. Rev.* **2012**, *112*, 3083–3135.  
55  
56  
57  
58  
59  
60

1  
2  
3 (31) Skinner, A. L.; Laurence, J. S. High-field solution NMR spectroscopy as a tool for  
4 assessing protein interactions with small molecule ligands. *J. Pharm. Sci.* **2008**, *97*, 4670–  
5 4695.  
6  
7  
8

9  
10  
11 (32) Powers, R. Advances in nuclear magnetic resonance for drug discovery. *Exp. Opin.*  
12 *Drug Discovery.* **2009**, *4*, 1077–1098.  
13  
14

15  
16 (33) Dömling, A. Small molecular weight protein–protein interaction antagonists—an  
17 insurmountable challenge? *Curr. Opin. in Chem. Biol.* **2008**, *12*, 281–291.  
18  
19  
20

21  
22 (34) Ding, Q.; Zhang, Z.; Liu, J.-J.; Jiang, N.; Zhang, J.; Ross, T.M.; Chu, X.-J.;  
23 Bartkovitz, D.; Podlaski, F.; Janson, C.; Tovar, C.; Filipovic, Z. M.; Higgins, B.; Glenn, K.;  
24 Packman, K. Discovery of RG7388, a potent and selective p53-MDM2 inhibitor in clinical  
25 development. *J. Med. Chem.* **2013**, *56*, 5979–5983.  
26  
27  
28  
29  
30

31  
32 (35) Graves, B.; Thompson, T.; Xia, M.; Janson, C.; Lukacs, C.; Deo, D.; Di Lello, P.; Fry,  
33 D.; Garvie, C.; Huang, K. S.; Gao, L.; Tovar, C.; Lovey, A.; Wanner, J.; Vassilev, L. T.  
34 Activation of the p53 pathway by small-molecule-induced MDM2 and MDMX dimerization.  
35 *Proc. Natl. Acad. Sci. U. S. A.* **2012**, *109*, 11788–11793.  
36  
37  
38  
39  
40

41  
42 (36) Surmiak, E.; Twarda-Clapa; A.; Zak, K. M.; Musielak, B.; Tomala, M. D.; Kubica,  
43 K.; Grudnik, P.; Madej, M.; Jablonski, M.; Potempa, J.; Kalinowska-Tluscik, J.; Dömling, A.;  
44 Dubin, G. Holak, T. A. A Unique Mdm2-binding mode of the 3-pyrrolin-2-one- and 2-  
45 furanone-based antagonists of the p53-Mdm2 interaction. *ACS Chem. Biol.* **2016**, *11*, 3310–  
46 3318.  
47  
48  
49  
50  
51  
52

53  
54 (37) Bista, M.; Kowalska, K.; Janczyk, W.; Dömling, A.; Holak, T. A. Robust NMR  
55 screening for lead compounds using tryptophan-containing proteins. *J. Am. Chem. Soc.* **2009**,  
56 *131*, 7500–7501.  
57  
58  
59  
60

1  
2  
3 (38) Oh, E. J.; Park, K.; Kim, K. S.; Kim, J.; Yang, J. A.; Kong, J. H.; Lee, M. Y.;  
4  
5 Hoffman, A. S.; Hahn, S. K. Target specific and long-acting delivery of protein, peptide, and  
6  
7 nucleotide therapeutics using hyaluronic acid derivatives. *J. Control. Release* **2010**, *141*, 2-12.  
8  
9

10  
11 (39) Czarna, A.; Popowicz, G. M.; Pecak, A.; Wolf, S.; Dubin, G.; Holak, T. A. High  
12  
13 affinity interaction of the p53 peptideanalogue with human Mdm2 and Mdmx. *Cell Cycle*  
14  
15 **2009**, *8*, 1176–1184.  
16  
17

18  
19 (40) Huang, X. Fluorescence polarization competition assay: the range of resolvable  
20  
21 inhibitor potency is limited by the affinity of the fluorescent ligand. *J. Biomol. Screen.* **2003**,  
22  
23 *8*, 34-38.  
24  
25

26  
27 (41) Showalter, S. A.; Bruschiweiler-Li, L.; Johnson, E.; Zhang, F.; Brüschiweiler, R.  
28  
29 Quantitative lid dynamics of Mdm2 reveals differential ligand binding modes of the p53-  
30  
31 binding cleft. *J. Am. Chem. Soc.* **2008**, *130*, 6472–6478.  
32  
33

34  
35 (42) Grace, C. R.; Ban, D.; Min, J.; Mayasundari, A.; Min, L.; Finch, K. E.; Griffiths, L.;  
36  
37 Bharatham, N.; Bashford, D.; Kiplin Guy, R.; Dyer, M. A.; Kriwacki, R. W. Monitoring  
38  
39 ligand-induced protein ordering in drug discovery. *J. Mol. Biol.* **2016**, *428*, 1290–1303.  
40  
41

42  
43 (43) Piotto, M.; Saudek, V.; Sklenár, V. Gradient-tailored excitation for single-quantum  
44  
45 NMR spectroscopy of aqueous solutions. *J. Biomol. NMR* **1992**, *2*, 661–665.  
46  
47

48  
49 (44) Mori, S.; Abeygunawardana, C.; Johnson, M. O.; van Zijl, P. C. Improved sensitivity  
50  
51 of HSQC spectra of exchanging protons at short interscan delays using a new fast HSQC  
52  
53 (FHSQC) detection scheme that avoids water saturation. *J. Magn. Reson. B* **1995**, *108*, 94–98.  
54  
55

56  
57 (45) Stoll, R.; Renner, C.; Hansen, S.; Palme, S.; Klein, C.; Belling, A.; Zeslawski, W.;  
58  
59 Kamionka, M.; Rehm, T.; Muhlhahn, P.; Schumacher, R.; Hesse, F.; Kaluza, B.; Voelter, W.;  
60

1  
2  
3 Engh, R. A.; Holak, T. A. Chalcone derivatives antagonize interactions between the human  
4  
5 oncoprotein MDM2 and p53. *Biochemistry* **2001**, *40*, 336–344.  
6  
7  
8  
9  
10

11 **TABLES, FIGURES AND FIGURE LEGENDS**  
12  
13  
14  
15  
16  
17  
18  
19  
20  
21  
22  
23  
24  
25  
26  
27  
28  
29  
30  
31  
32  
33  
34  
35  
36  
37  
38  
39  
40  
41  
42  
43  
44  
45  
46  
47  
48  
49  
50  
51  
52  
53  
54  
55  
56  
57  
58  
59  
60

**Table 1.** Inhibitory activities of compound **1** and its derivatives against the p53-MDM2/MDMX interaction using the FP assay.

Code	R <sub>2</sub>	K <sub>i</sub> M2 [μM]	K <sub>i</sub> MX [μM]	Code	R <sub>2</sub>	K <sub>i</sub> M2 [μM]	K <sub>i</sub> MX [μM]
<b>1</b> *		0.006	3.15	<b>13</b>		0.121	n.a.#
<b>2</b>		0.225	n.a.	<b>14</b>		0.017	40.2
<b>3</b>		0.023	14.7	<b>15</b>		0.059	n.a.
<b>4</b>		0.038	29.6	<b>16</b>		0.015	9.75
<b>5</b>		2.31	n.a.	<b>17</b>		0.098	n.a.
<b>6</b>		0.038	n.a.	<b>18</b>		0.054	12.4
<b>7</b>		28.0	n.a.	<b>19</b>		0.058	26.3
<b>8</b>		0.008	35.3	<b>20a</b> <sup>±</sup>		6.02	n.a.
<b>9</b>		0.656	27.4	<b>20</b> <sup>°</sup>		0.021	4.91
<b>10</b>		n.a.	n.a.	<b>21a</b>		n.a.	n.a.
<b>11</b>		n.a.	n.a.	<b>21</b>		0.060	4.40
<b>12</b>		n.a.	n.a.	<b>22a</b>		n.a.	n.a.
				<b>22</b>		0.433	4.71
				<b>23a</b>		n.a.	n.a.
				<b>23</b>		0.322	6.76
				<b>24a</b>		n.a.	n.a.
				<b>24</b>		0.157	4.17

\*compounds **1-19** have 4-chlorophenyl group in R<sub>1</sub> position; °compounds **20-24** have hydroxyl group in R<sub>2</sub> position; <sup>±</sup>**a** stands for ethyl ester (**20a-24a**) of the respective acidic forms of **20-24**; #n.a. stands for not active.

**Table 2.** Selectivity of the tested compounds towards the p53 positive cells. IC<sub>50</sub> values were obtained from the MTT assay. Selectivity is calculated as a ratio of IC<sub>50</sub> values towards the p53 negative (Saos-2) and positive (U-2 OS) cells.

Code	U-2 OS IC <sub>50</sub> [μM]	Saos-2 IC <sub>50</sub> [μM]	Selectivity
<b>19</b>	11.08 ± 1.83	38.56 ± 3.61	3.48
<b>1</b>	17.42 ± 3.49	55.82 ± 13.49	3.20
<b>16</b>	5.71 ± 1.39	12.73 ± 2.66	2.23
<b>13</b>	3.67 ± 0.28	7.15 ± 1.33	1.95
<b>14</b>	7.27 ± 0.63	11.69 ± 1.30	1.61
<b>Nutlin-3</b>	2.66 ± 0.39	20.16 ± 4.71	7.59

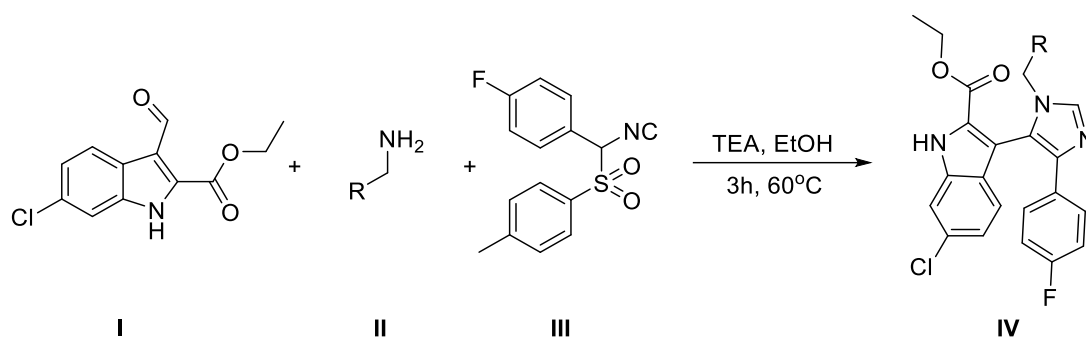


**Figure 1.** The Van Leusen reaction used for the synthesis of the series scaffold. The substituents are varied by changing the amine and isocyanide components (for details see the SI).



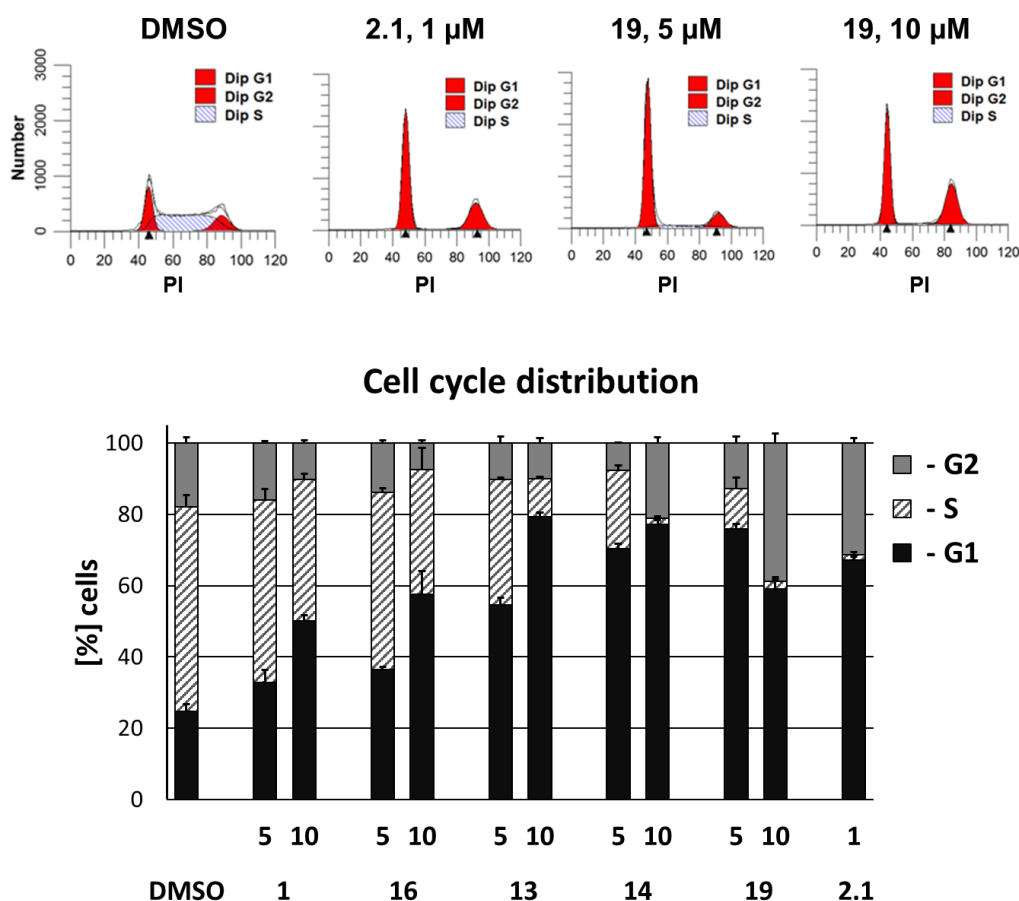


**Figure 3.** Compound **19** induces cell cycle arrest in the U-2 OS (p53<sup>+/+</sup>) cells. The cells were treated with DMSO, 5 or 10 μM of the tested compounds, or with 1 μM of **2.1** (positive control) for 24 h. The cells were fixed and stained with propidium iodide, followed by flow cytometry analysis of DNA content. Upper panel: exemplary histograms. Lower panel: Cell cycle distribution shown as the mean ± SD of two independent experiments.

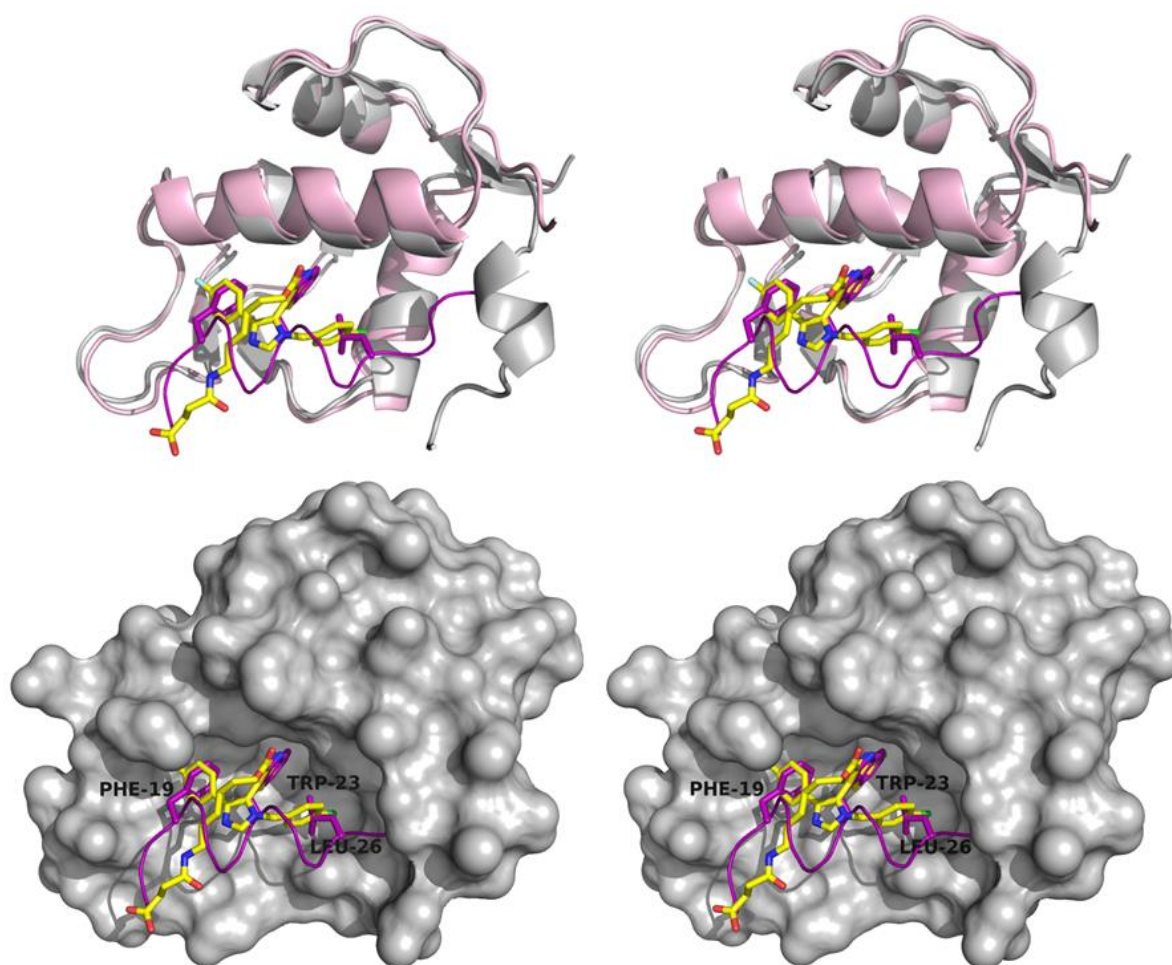


**Figure 4.** Interaction of MDM2 (residues 18-125) with **19** in comparison with the MDM2-p53 peptide complex (PDB ID: 1YCR). Stereoviews in cartoon (upper panel) or surface representations (lower panel) are shown. MDM2 from the MDM2-**19** complex is shown in grey, whereas from the MDM2-p53 complex – in pink. **19** is shown as yellow sticks, the p53 peptide – as a violet ribbon with the three key interacting amino acids depicted as sticks.

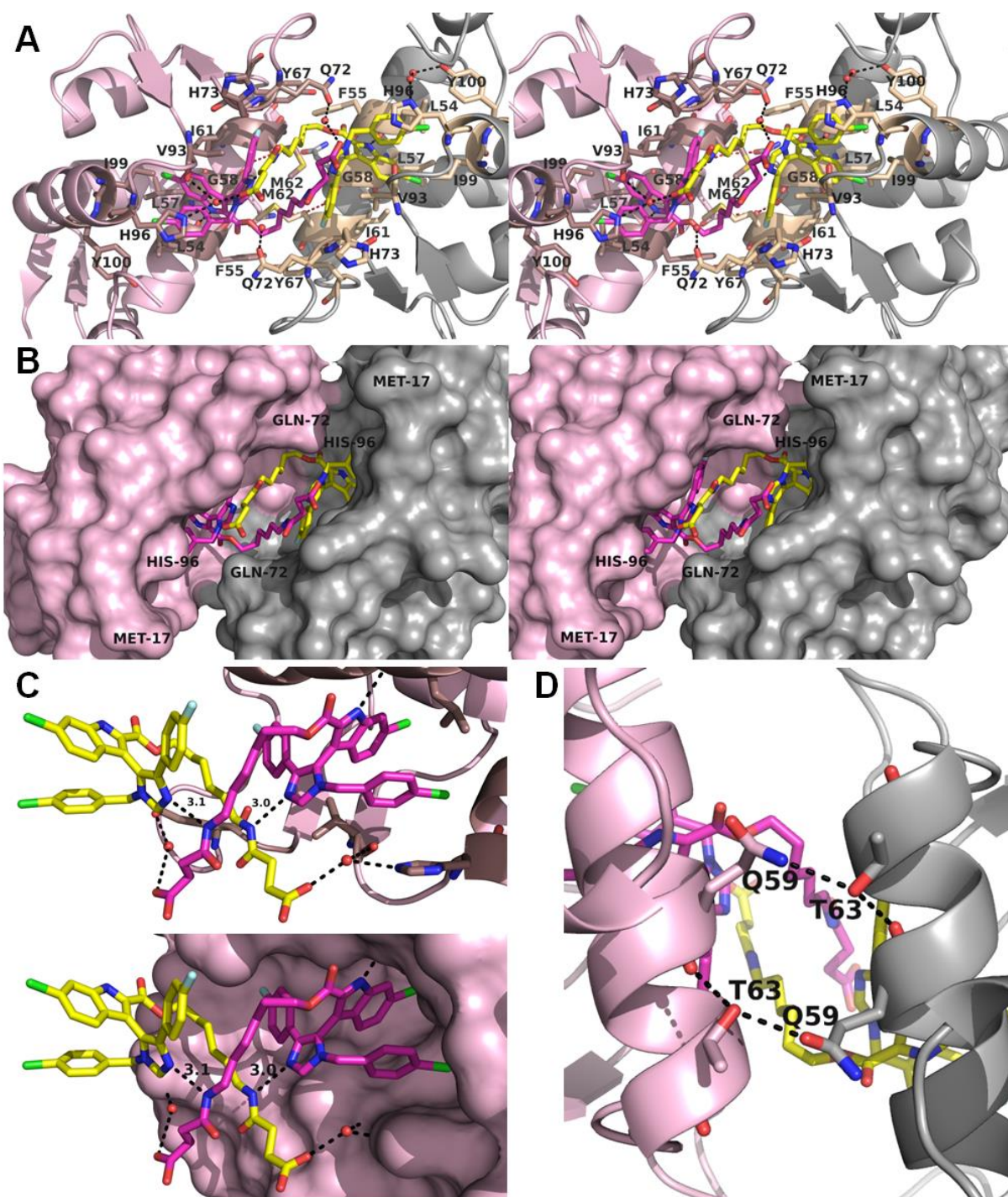


**Figure 5.** Crystal structure reveals the **19**-induced dimerization of MDM2. A. Stereoview of the structure of the MDM2(18-125)-**19** complex. MDM2 chains A (pink) and B (grey) are shown in the cartoon representation. Inhibitors are shown as magenta and yellow sticks. Residues involved in the interactions with **19** are shown as sticks in salmon (chain A) or wheat (chain B) and labeled. Hydrogen bonds contributed by the inhibitors are depicted as black dashes. B. Stereoview of the MDM2(18-125)-**19** complex – surface representation.

1  
2  
3 Orientation and color coding same as in panel A. C. Inter-inhibitor interactions – the close-up  
4 view of the MDM2 binding pocket shown as a pink cartoon (upper panel) or surface (lower  
5 panel) with the buried inhibitor molecule and adjacent inhibitor molecule. The second MDM2  
6 molecule within the dimer is not shown. Hydrogen bonds are highlighted. D. Direct protein-  
7  
8 protein intermonomer interactions are formed between  $\alpha$ -helices of the adjacent MDM2  
9  
10 molecules. The interacting residues are shown as sticks; hydrogen bonds are highlighted in  
11  
12  
13  
14  
15  
16  
17  
18 black.  
19  
20  
21  
22  
23  
24  
25  
26  
27  
28  
29  
30  
31  
32  
33  
34  
35  
36  
37  
38  
39  
40  
41  
42  
43  
44  
45  
46  
47  
48  
49  
50  
51  
52  
53  
54  
55  
56  
57  
58  
59  
60

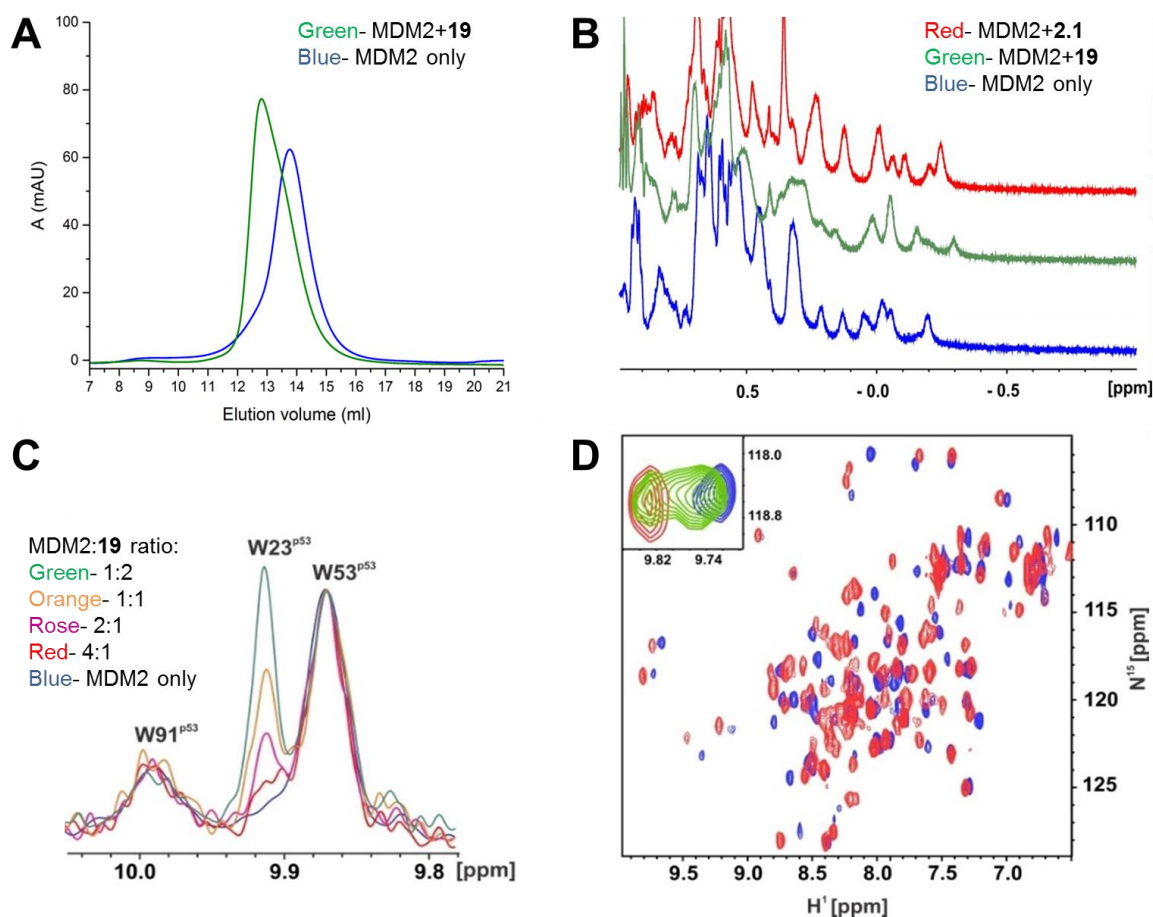


**Figure 6.** Compound **19** induces dimerization of MDM2 in solution and dissociates the MDM2-p53 complex. A. Increased retention time of MDM2 in analytical gel filtration in the presence of **19** indicates formation of the dimer. B. The aliphatic region of  $^1\text{H}$  NMR spectra of MDM2(18-125) in the 1:1 complex with indicated compounds. **2.1** binds MDM2, but does not induce dimer formation. Broadening of NMR resonance peaks in the MDM2-**19** complex indicates the MDM2 dimerization. C. 1D AIDA NMR. The selected region of the 1D NMR spectrum is shown, containing resonances originating from W23, W53 and W91 of p53. The W23 peak is not present in the spectrum of the p53-MDM2 complex, but is recovered after addition of **19**, indicating compound induced dissociation of the complex. D. The HSQC spectrum of the  $^{15}\text{N}$ -labeled MDM2 (blue) superimposed with the spectrum after addition of **16** in the 1:1 molar ratio (red). The inset shows an intermediate state of a selected peak at the MDM2:**16** molar ratio equal to 2:1 (green). NMR signal splitting indicates strong interaction at  $K_D$  below  $1\ \mu\text{M}$ .

## TABLE OF CONTENTS GRAPHIC

